Journal of Himalayan Earth Sciences Volume 58, No. 2, 2025 pp. 28-47

Delineating the Fluvial Channel System in B-Sand of NIM Block in Lower Indus Basin, Pakistan, using 3D seismic attributes

Furqan Mahmud Butt [1, 2*], Shazia Naseem [1, 3], and Umair Bin Nisar [2]

[1] Department of Earth Sciences, Quaid-e-Azam University, Islamabad, Pakistan
[2] Department of Meteorology, COMSATS University Islamabad, Islamabad, Pakistan
[3] Institute of Geophysics and Geomatics (IGG), China University of Geosciences (CUG), China
**Corresponding Author: furqanmahmud@yahoo.com*

Submitted Date: 23/04/2025 Acceptance Date: 24/06/2025 Publication Date: 30/11/2025

Abstract

Seismic attributes have emerged as indispensable tools in hydrocarbon exploration, facilitating the identification and characterization of subsurface reservoirs, including fluvial channel systems. These attributes enhance the interpretation of seismic data by extracting quantitative geological and petrophysical information. This study focuses on the B-Sand reservoir within the Cretaceous Lower Goru Formation in the NIM Block of the Lower Indus Basin, Pakistan, which is a proven hydrocarbon-bearing interval. Using integrated seismic and well log data, we analyzed four key seismic attributes, which are sweetness, trace envelope (TE), relative acoustic impedance (RAI), and root mean square (RMS) amplitude, to delineate fluvial channels and assess reservoir potential. Well log interpretations confirm two dominant lithologies within the B-Sand reservoir: sandstone and shale. Seismic mapping reveals a single prominent horizon and four faults, indicative of a step-faulting structural regime. Sweetness highlights high-amplitude zones, correlating with potential hydrocarbon-saturated sand units. RAI analysis effectively discriminates lithological variations, while TE attributes suggest possible gas accumulations. RMS Amplitude further corroborates hydrocarbon indicators, reinforcing the reservoir's prospectivity. The synergistic application of these attributes demonstrates significant hydrocarbon potential within the B-Sand reservoir, justifying further exploration. This approach provides a robust workflow for reservoir characterization in analogous fluvio-deltaic systems.

***Keywords*:** Post-stack attributes; B-Sand reservoir; NIM Block; Hydrocarbon Prospects; Gas-bearing sand zones

1. Introduction

Seismic interpretation provides initial discrimination between hydrocarbon and non-hydrocarbon bearing sands, yet cannot definitively identify fluid content (Khalid and Ghazi, 2013). This limitation necessitates advanced analytical workflows incorporating seismic attributes - mathematical transformations that extract subtle subsurface features (Taner, 2001). These attributes have evolved significantly since their inception (Hart and Balch, 2000), now offering both qualitative and quantitative insights into reservoir properties (Dorn, 1999), particularly in reducing parameter uncertainty (Zahmatkesh et al., 2018).

Attribute analysis operates across four seismic domains (time, amplitude, phase, frequency) and two implementation approaches (horizon-based and volumetric) (Brown, 2011; Dorn, 1999). This framework enables comprehensive reservoir characterization from depositional features to basin-wide trends. The methodology proves particularly valuable in fluvial systems, where complex depositional architectures and spatial variability present unique

challenges (Bridge and Tye, 2000). While these systems host substantial hydrocarbons (Zhang et al., 2011), their economic viability depends on accurately predicting sand geometry (Hong et al., 2013), making paleochannel identification crucial (Anees et al., 2019).

Sand deposits associated with fluvial and marine channels frequently constitute hydrocarbon reservoirs, rendering their detection a critical objective in seismic interpretation for exploration (Chopra and Marfurt, 2013). Seismic attributes enhance and quantify features of interest in both pre-stack and post-stack data, providing precise delineation of geologic structures and reservoir properties. When processed with amplitude-preserving workflows, lateral amplitude variations reflect key geological parameters, including porosity, lithology, and thickness variations (Chopra and Marfurt, 2013). Among the principal applications of seismic attributes are the identification of direct hydrocarbon indicators (DHIs), geometric edge-detection for structural boundaries, and physical attribute analysis for litho-fluid discrimination (Khalid et al., 2014). However, distinguishing payable hydrocarbon intervals from non-productive zones remains challenging using seismic data alone (Khalid and Ghazi, 2013), necessitating integrated methodologies.

To refine reservoir characterization, amplitude-derived attributes—such as root mean square (RMS) and sweetness—are employed. Sweetness, in particular, aids in differentiating sand bodies, shale layers, and channel geometries, elucidating both lateral and vertical heterogeneities within target intervals (Raef et al., 2015).

Despite extensive studies on the Lower Goru Formation, significant reservoir potential remains untapped due to an insufficient understanding of sand dispersal patterns. Conventional seismic data often exhibit composite reflections at reservoir zones, a consequence of low-velocity overlying shale, which obscures interpretation (Krois et al., 1998). High-resolution seismic data are thus essential to resolve interbedded shale-sand sequences. Previous reservoir assessments have predominantly relied on petrophysical analyses (Azeem et al., 2017), neglecting critical facies evaluation. Although recent work (Ali et al., 2018) applied post-stack inversion algorithms to characterize reservoir properties, a holistic integration of seismic, facies, and production data has yet to be implemented.

This study advances reservoir classification by petrophysical analysis, synthesizing facies analysis and 3D seismic attribute interpretation. We delineate the lateral and vertical facies distribution of the Lower Goru Formation, with emphasis on the B-sand interval in the NIM Exploration Block. By correlating well log facies with 3D seismic attributes, we reconstruct depositional environments and sand-shale distributions. Furthermore, production data are incorporated to validate spatial sweet-spot predictions derived from seismic slices and well logs, establishing a robust prospect evaluation framework.

2. Geology/Area of Study

Pakistan occupies a critical position at the triple junction of the Arabian, Indian, and Eurasian tectonic plates, making its geological evolution particularly complex. About 200 million years ago, the Indian Plate, which had been a part of the supercontinent Gondwana, started moving northward and eventually merged with the Eurasian Plate 40–50 million years ago (Ahmed et al., 2014). This continental fragment migrated northward at 3-5 cm/year, traversing the equator before its collision with the Eurasian Plate during the late Palaeocene to Eocene (Ahmed, 2018). This continental convergence initiated the Himalayan orogeny, fundamentally shaping the region's modern geological architecture (Abbasi et al., 2015a, b; Bilal et al., 2022; Knight et al., 2023).

The sedimentary succession of the Lower Indus Basin contains several economically significant formations, most notably the Sember and Lower Goru Formations (Fig. 1). These units comprise a complex stratigraphy of alternating sandstones and shales, including the Upper Sand, Upper Shale, Middle Sand, Lower Shale, Basal Sand, Talhar Shale, and Massive Sand members (Ahmed et al., 2018). The Upper Sand demonstrates reservoir potential, being subdivided into four distinct units (A-D sands) characterized by exceptional porosity preservation despite hydrocarbon migration from the Sember Formation source rocks (Schenk et al., 2017). This petroleum system is further complicated by the conformable contact between the Sember Formation and the underlying Chiltan Limestone, which serves as both a reservoir and potential migration pathway (Khalid et al., 2018).

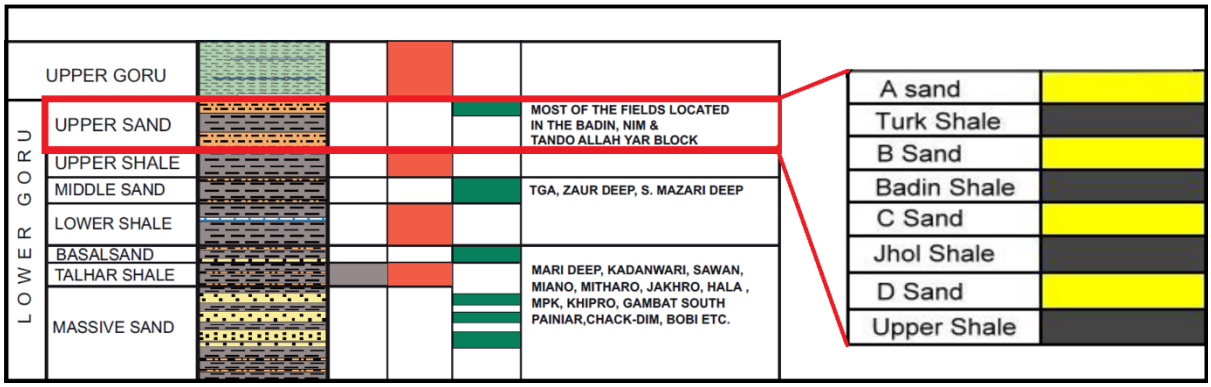

Fig. 1. Lower Goru Formation within the generalized stratigraphy of the Lower Indus Basin (marked by red rectangle) (modified after Baig et al., 2016).

Exploration history in the Indus Basin reveals its substantial hydrocarbon potential. Union Texas Petroleum's groundbreaking exploration efforts between 1977 and 1997 produced 49 important hydrocarbon discoveries in the Lower Goru Formation, starting with the first commercial success in 1981 (Abbasi et al., 2015b). The NIM Block, encompassing 235.26 km² in Hyderabad and Tando Allahyar districts, exemplifies current exploration frontiers in this mature petroleum province. Operated by a consortium led by OGDCL (95% interest) and GHPL (5%), this block's position within the southern Sindh Monocline places it in a strategic location for further hydrocarbon discoveries (Ahmed et al., 2014). The geological setting of the block, combined with an advanced understanding of the tectonic evolution of the basin and petroleum systems, suggests considerable untapped potential remains in this structurally complex region (Fig. 2).

3. Data Sets

The seismic and well log datasets utilized for this study were obtained from the Directorate General of Petroleum Concessions (DGPC), Pakistan, and Landmark Resources (LMKR), Islamabad, Pakistan. The 3D seismic dataset used for this study comprises about 15 km^2 of data organized in an orderly 116 in-lines (53-169) and 158 cross-lines (189-347).

4. Methodology

This study employed an integrated workflow combining well log data and seismic measurements to generate a synthetic seismic section (Fig. 3), which established precise time-depth relationships for stratigraphic horizons. Petrophysical analysis, heavily reliant on well log data, is an integral part of reservoir characterization. The initial assessment provides parameters such as porosity, permeability, fluid saturation, and shale volume. Building on these results, four key seismic attributes (Sweetness, TE, RAI, and RMS Amplitude)

were applied to identify hydrocarbon zones, lithologic variations, and channel geometries. The synergistic use of petrophysical data and seismic attributes significantly improved structural and stratigraphic interpretation accuracy, enabling reliable reservoir classification and hydrocarbon potential assessment. This comprehensive methodology reduced interpretation uncertainties while providing critical insights for future exploration and development strategies in complex reservoir environments.

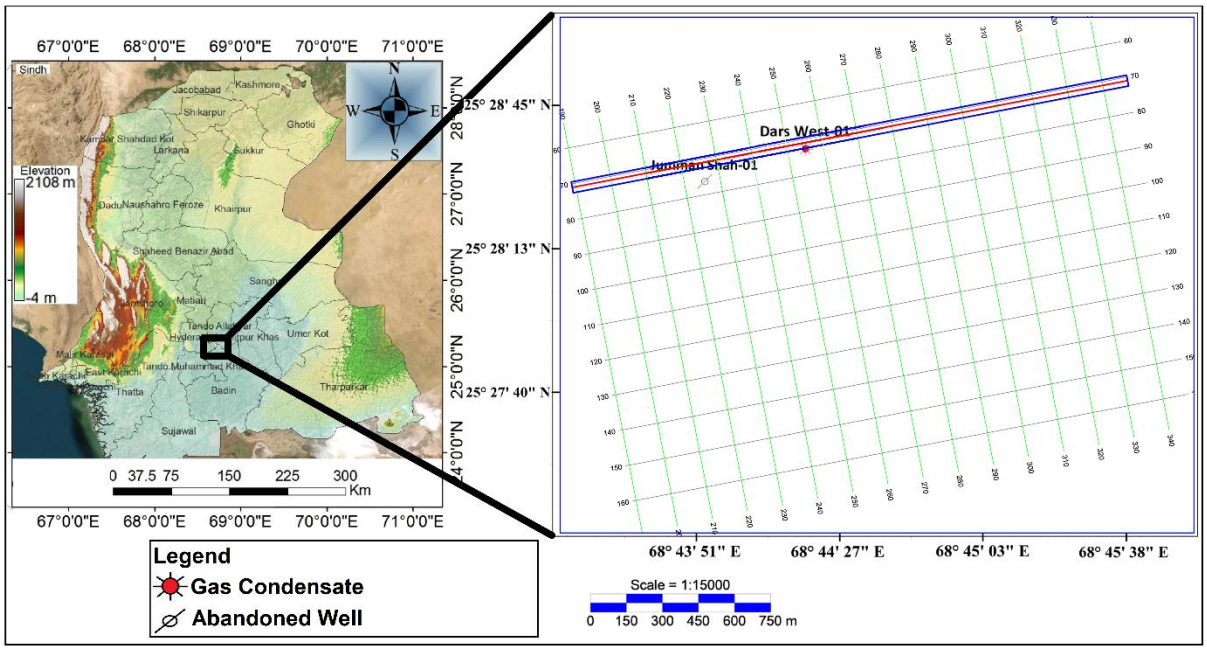

Fig. 2. a) Elevation Map of Sindh, Pakistan (Zehra and Afsar, 2016), **b)** Base map of NIM Block with the location of wells.

5. Methodology

This study employed an integrated workflow combining well log data and seismic measurements to generate a synthetic seismic section (Fig. 3), which established precise time-depth relationships for stratigraphic horizons. Petrophysical analysis, heavily reliant on well log data, is an integral part of reservoir characterization. The initial assessment provides parameters such as porosity, permeability, fluid saturation, and shale volume. Building on these results, four key seismic attributes (Sweetness, TE, RAI, and RMS Amplitude) were applied to identify hydrocarbon zones, lithologic variations, and channel geometries. The synergistic use of petrophysical data and seismic attributes significantly improved structural and stratigraphic interpretation accuracy, enabling reliable reservoir classification and hydrocarbon potential assessment. This comprehensive methodology reduced interpretation uncertainties while providing critical insights for future exploration and development strategies in complex reservoir environments.

5.1 Petrophysics

Shale formations exhibit higher natural radioactivity compared to arenaceous or carbonate lithologies. The volume of shale (V_{sh}) within sandstone or carbonate reservoirs serves as a crucial parameter in petrophysical evaluation (Mehana and El-Monier, 2016). V_{sh} is typically quantified using the gamma ray (GR) log, employing the linear interpolation method as formulated by Asquith and Gibson (1982).

$$V_{sh} = \frac{(GR - GR_{min})}{(GR_{max} - GR_{min})} \quad (1)$$

Where GR_{max} and GR_{min} represent the maximum and minimum gamma ray readings, respectively, measured in American Petroleum Institute (API) units.

Porosity in subsurface formations, representing the void space available for fluid storage, is fundamentally related to the lithological matrix, bulk density (RHO_b), and fluid density (RHO_f). The density log-derived porosity (PHID) can be estimated using the following relationship (Foster and Beaumont, 1999).

$$PHID = \frac{(RHO_{ma} - RHO_b)}{(RHO_b - RHO_f)} \quad (2)$$

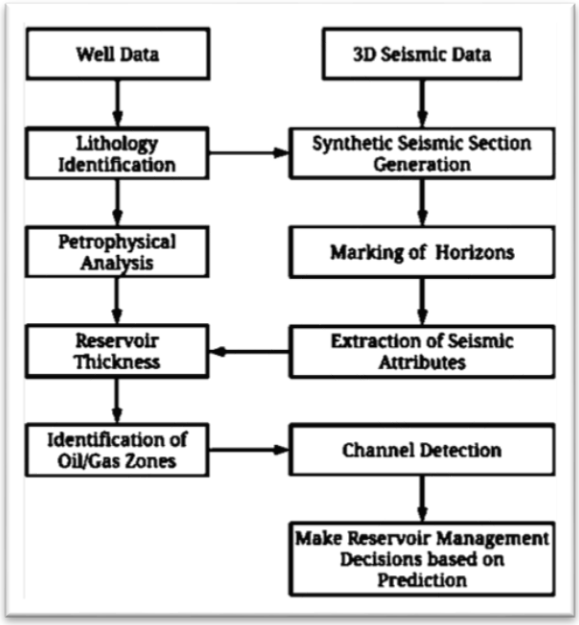

Fig. 3. Workflow used in this study to differentiate gas-bearing sand from non-gas-bearing sand intervals.

Here, RHO_{ma} denotes the matrix density of the formation, RHO_b is the bulk density obtained from well logs, and RHOf represents the density of the fluid saturating the pore space proximal to the wellbore.

Effective porosity (PHIE), which represents the interconnected pore volume available for fluid flow, is derived by subtracting the porosity associated with shale or clay-bound water from the total porosity. A common empirical approach for its calculation (Owolabi, 2019) incorporates neutron porosity (NPHI).

$$PHIE = \frac{(PHID + NPHI)}{2} \times (1 - V_{sh}) \quad (3)$$

The Hydrogen Index (HI) of a reservoir rock, indicative of its hydrogen content, is related to its porosity. Neutron porosity measurements, obtained using a neutron source, are sensitive to the hydrogen nuclei present in the formation fluids. HI is defined as the ratio of the hydrogen atom density in a sample to that of pure water at approximately 23°C. The intensity of neutron interactions can thus be utilized to estimate the volume of liquid-filled porosity (Asquith et al., 2004).

Sonic porosity (PORS) is determined from the interval transit time of compressional waves through the formation. The Wyllie time-average equation (Wyllie *et al.*, 1956) provides a widely used method for its computation.

$$PORS = \frac{\Delta t_{log} - \Delta t_{matrix}}{\Delta t_f - \Delta t_{matrix}} \quad (4)$$

Where Δt_{log} is the interval transit time measured by the sonic log, Δt_{matrix} is the interval transit time of the rock matrix, and Δt_f is the interval transit time of the interstitial fluid, all expressed in microseconds per foot (µs/ft) or seconds per meter (s/m).

Water saturation (S_w), representing the fraction of the pore volume occupied by water, is a fundamental parameter in reservoir evaluation. The Archie equation (Archie, 1942) provides an empirical relationship for its estimation:

$$S_w = \left\{\frac{A \times R_w}{PHIE^m \times R_t}\right\}^{\frac{1}{N}} \quad (5)$$

Where A is the tortuosity factor, M is the cementation exponent, N is the saturation exponent, R_t is the resistivity of the formation, and R_w is the resistivity of the formation water.

Hydrocarbon saturation (Shc), the proportion of the pore volume occupied by hydrocarbons, can be directly derived from water saturation (Dake, 1983):

$$S_{hc} = 1 - S_w \quad (6)$$

5.2 Sweetness Attribute

The Sweetness attribute, derived from seismic data, is employed to identify potential hydrocarbon-bearing zones, often referred to as "sweet spots." It is mathematically defined as the ratio of the seismic amplitude to the square root of the instantaneous frequency (Barnes, 2016):

$$S_r(t) = \frac{a_r(t)}{\sqrt{f_r(t)}} \quad (7)$$

This attribute aids in the delineation of stratigraphic features, particularly channel systems, by integrating information from reflection strength and instantaneous frequency (Hart, 2008).

5.3 Relative Acoustic Impedance (RAI)

Acoustic impedance (I) is a fundamental physical property of subsurface materials, defined as the product of density (ρ) and compressional wave velocity (V):

$$I = \rho V \quad (8)$$

Seismic inversion techniques are utilized to transform seismic reflection data into an acoustic impedance model. Relative Acoustic Impedance (RAI) can be quantified by considering the real component of the reference signal from the seismic trace (Taner, 2000). Seismic inversion is predicated on the assumption of a reduced signal-to-noise ratio and processed data containing a broadband, zero-phase wavelet (Abbasi et al., 2016; Emujakporue and Enyenihi, 2020; Daber et al., 2007). The reflection coefficient f(t) can be approximated as:

$$f(t) = \frac{1}{2}\frac{\Delta\rho V}{\rho V} \quad (9)$$

Integrating this expression yields the natural logarithm of the acoustic impedance:

$$\ln(\rho V) = 2\int_{t=0}^{t=T} f(t)\,dt \quad (10)$$

Where f(t) represents the seismic trace. RAI is typically generated by aggregating the acoustic impedance attribute over a specified time window (Alsouki et al., 2014). Low-frequency noise in seismic data can introduce long-wavelength artefacts, potentially skewing the results. Bandpass or low-cut filters are commonly applied during seismic data processing to mitigate this issue (Abbasi et al., 2016; Emujakporue and Enyenihi, 2020). Variations in the integrated acoustic impedance map are indicative of changes in lithology, density, porosity, and other reservoir characteristics, making this attribute a valuable tool for reservoir characterization (Taner et al., 1979).

5.4 Trace Envelope (TE) Attribute

The Trace Envelope (TE), also known as instantaneous amplitude, is a seismic attribute that represents the magnitude E(t) of a seismic trace s(t). It is computed as the modulus of the complex seismic trace, reflecting the total instantaneous energy, independent of phase (Taner et al., 1979). The TE of a seismic signal can highlight individual interface reflections or the composite response of multiple interfaces, depending on the seismic bandwidth. The amplitude of the trace at any given time t is determined by:

$$E(t) = \sqrt{\left(R_e\, s(t)\right)^2 + (I_m s(t))^2} \quad (11)$$

Where Re(s(t)) is the real part of the analytic seismic trace (the original seismic trace), and $I_m(s(t))$ is the imaginary part, obtained through the Hilbert transform of Re(s(t)), also known as the quadrature trace.

5.5 Root Mean Square (RMS) Attribute

The Root Mean Square (RMS) amplitude is an important seismic attribute

directly associated with properties of the reservoir and stratigraphic elements. The RMS value represents the average energy in a defined time window of the seismic trace (Azeem et al., 2016). Mathematically, the RMS Amplitude is given by:

$$\mathrm{RMS} = \sqrt{\frac{1}{\mathrm{N}}\sum_{\mathrm{i}=1}^{\mathrm{N}} \mathrm{A(i)}^2} \qquad (12)$$

Where N represents the number of samples within the analysis window and A(i) denotes the amplitude of the i^{th} sample. This formulation inherently makes RMS amplitude particularly sensitive to high amplitude values, as individual amplitudes are squared before averaging, thereby accentuating their contribution to the overall energy estimation. This sensitivity allows RMS amplitude to effectively highlight significant impedance contrasts often associated with hydrocarbon accumulations or distinct lithological boundaries.

6. Results

6.1 Marking of Horizon and Identification of Faults

The correlation and identification of the horizon B-Sand were carried out thoroughly by combining existing well data formation tops with a synthetic seismogram (Fig. 4). This was done starting with the calibration of the digitized bulk density and sonic logs to the 3D seismic. In particular, well data of Jumman Shah-01 was used for the creation of the synthetic seismogram. A wavelet was retrieved from the seismic data, in the span of a target window between 1534m and 1618m, exactly from the inline and cross-line seismic traces. The obtained wavelet was subsequently convolved with the reflectivity series converted from the sonic and density logs to generate a synthetic seismogram. Following the depth-to-time conversion of the obtained seismogram using check shot data. The synthetic seismogram and seismic traces were subsequently accurately calibrated to build an impedance model in the form of a series of reflection coefficients. An Ormsby wavelet was used for this dataset, which has a 0.002-second sample rate, frequency bounds of 5, 10, 60, and 90 Hz, and a 0.4-second sample length. Figure 5 shows the well-to-seismic tie with the synthetic seismogram, reflectivity series, and the extracted wavelet calculated from it, with the B-Sand formation well indicated in red. Additional structural analysis on the seismic data (Fig. 5) established four separated normal faults (Fault-1, Fault-2, Fault-3, and Fault-4), suggestive of an extensional regime in the region.

6.2 Petrophysical Analysis

Petrophysical analysis of Jumman Shah-01 and Dars West-01 well logs has facilitated the identification and characterization of the B-Sand as a zone of hydrocarbon accumulation. The petrophysical parameters derived from calculations are tabulated in Table 1, with detailed interpretations displayed in Figs. 6 and 7 for Jumman Shah-01 and Dars West-01, respectively.

V_{sh} was calculated to evaluate the lithological composition of the reservoir interval. With a Gamma Ray (GR) log cut-off of 85 API used as the separator for sand and shale, V_{sh} values of around 18% for Jumman Shah-01 and 20% for Dars West-01 were estimated (Table 1).

Table 1: Petrophysical values of parameters in B-Sand encountered in wells under study.

Sr. no.	Well Name	Depth (m)	V_{sh} (%)	PHID (%)	PHIE (%)	PORS (%)	S_w (%)	S_{hc} (%)
1	Dars West-01	1852-1944	20.5	18.6	11.0	18.42	43.7	56.30
2	Jumman Shah-01	1534-1618	18.6	22.6	16.98	22.48	79.75	20.25

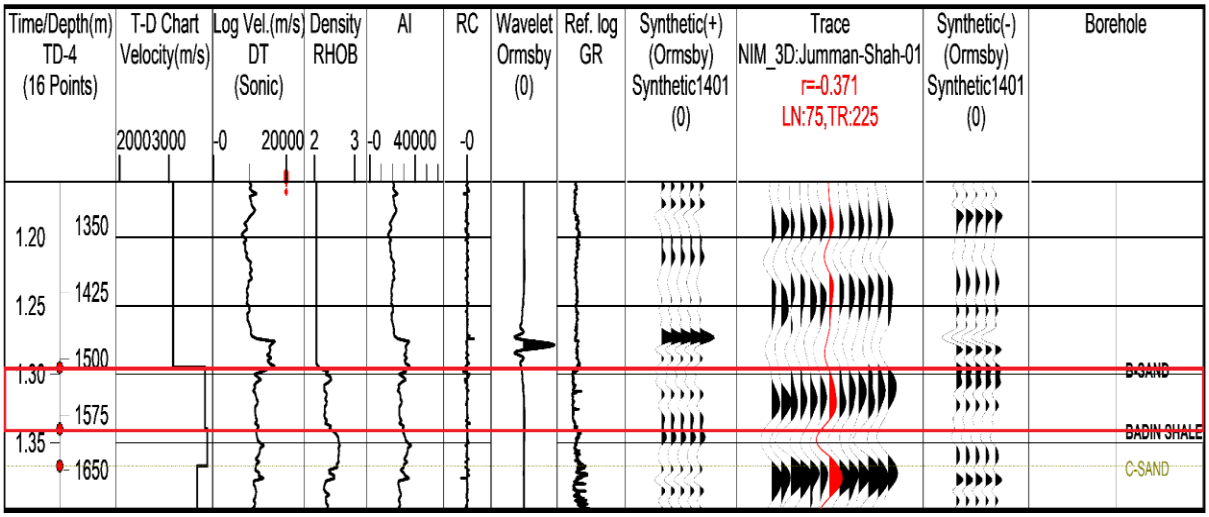

Fig. 4. Synthetic seismogram derived from the data of well Jumman Shah-01.

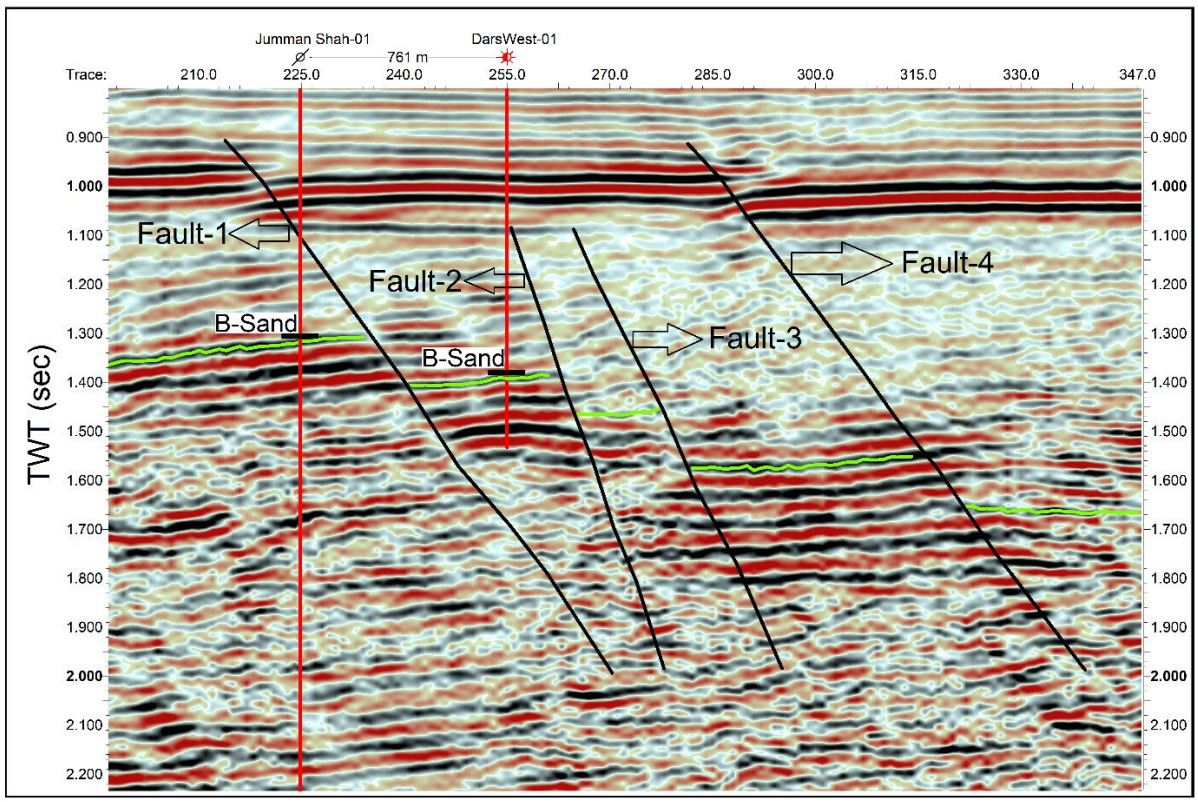

Fig. 5. Seismic section (In-line 71, as shown in Figure 2) presenting the marked B-Sand (Green) with Two Way Time (TWT) of 1.3 sec, Faults (Black), and Well (Red).

Such low volumes of shale suggest that the B-Sand in both the wells consists largely of sand with thin shale interbeds. Further study of porosity indicates good reservoir quality. In Jumman Shah-01, total porosity (PORS) and effective porosity (PHIE) are close to 22% and 16%, respectively, whereas in Dars West-01, these are close to 18% and 11%. Such porosity indicates fair to good quality reservoir sands in both wells (Figs. 6 and 7). Lastly, water saturation (S_w) was computed to analyze fluid content. In Jumman Shah-01, S_w is more than 79%, reflecting high-water concentration in the reservoir, even if its porosity is fair to good. In Dars West-01, S_w

is more than 43%, reflecting comparatively higher hydrocarbon concentration, although the reservoir is water-wet.

6.3 Delineation of Fluvial Channels within the B-Sand

Seismic attribute analysis is applied in this research to define the occurrence, spatial distribution, and stratigraphic architecture of fluvial channel systems in the study area. Attribute maps not only validate the occurrence of these channels but also give in-depth information regarding the dimensional attributes, lateral continuity, and vertical stacking (Fig. 8). The channels seen have considerable morphological complexity due to varying erosional regimes, sediment supply dynamics, changes in flow velocity, and localized tectonic effects.

The volumes taken across the B-Sand Formation show well-defined reflection amplitudes (illustrated in red to yellow colors), reflecting high-impedance contrasts, which are stratigraphically separated by low-reflectivity shale beds (indicated in blue to black). Three different fluvial channels have been found in the study area: two of them show sinuous, meandering geometries, whereas the third one has a linear shape (Fig. 8). Hydrodynamic modelling of the channels shows that the outer banks are subjected to constant flow velocities, which enhance erosional undercutting, while the inner banks exhibit low velocities, which aid sediment deposition and formation of point-bar sequences. The meandering channels cover lengths of around 15 km and 28 km, respectively, and the central channel is 1.1 km in length with varying widths ranging from 110 m to 130 m.

In addition, structural interpretation demonstrates four normal faults, defined by high-frequency seismic discontinuities (Fig. 8). These faults are interpreted to represent vital conduits for hydrocarbon migration, presumably enhancing fluvial-derived reservoir facies entrapment. There is a high correlation between these fault systems and the related geomorphic features, as supported by vertical seismic amplitude analysis.

Stratigraphically, the B-Sand Formation has several shale-filled channel complexes, which traverse the floodplain and function as regional seal rocks. These are tectonically held in by fault-bounded point-bar sandstone deposits, some of which can form stratigraphic hydrocarbon traps (Fig. 8). This verifies the dominance of sand-rich facies (red to yellow) in the channel fills, interbedded with subordinate shale units (blue to light blue).

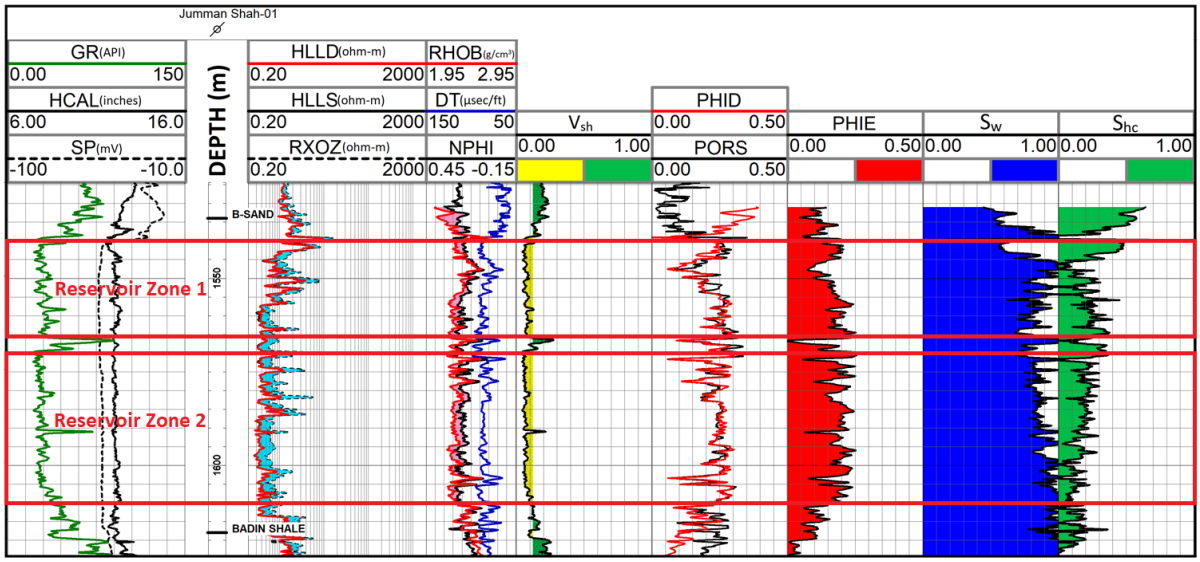

Fig. 6. Petrophysical Interpretation of B-Sand in Jumman Shah-01 with all the calculations of V_{sh}, PHID, PHIE, PORS, S_w, and S_{hc}.

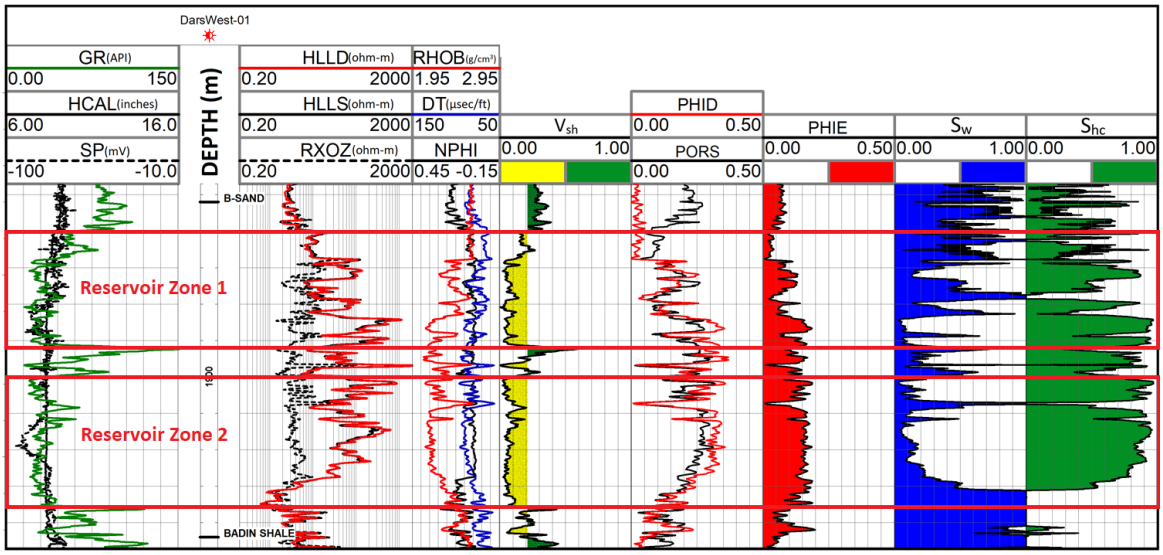

Fig. 7. Petrophysical Interpretation of Dars West-01 with all the calculations of V_{sh}, PHID, PHIE, PORS, S_w, and S_{hc}.

6.4 Sweetness Attribute

The seismic sweetness attribute was employed to evaluate the productive zones within the B-Sand horizon, revealing distinct reservoir characteristics. High sweetness values (red-orange) in the northeastern (NE) and southwestern (SW) sectors indicate favorable hydrocarbon-bearing intervals, while lower values (blue-black) correspond to less prospective zones (Fig. 9). The horizon slice delineates a prominent fault system comprising four major faults, which significantly influence reservoir geometry and fluid distribution. Sediment influx predominantly controls depositional architecture, with channel and point bar facies identified through fining-upward gamma-ray (GR) log signatures.

The correlation between high sweetness attributes and channel-fill/point bar deposits confirms gas-saturated zones, validated by wells Jumman Shah-01 and Dars West-01 (Fig. 10). Petrophysical analysis reveals that Jumman Shah-01, despite higher sweetness values, was abandoned due to elevated water saturation, whereas Dars West-01 penetrated deeper into the Chiltan Formation. The B-Sand is interpreted as a fluvial-dominated system with enhanced porosity and permeability at its base, evidenced by low GR responses.

A prospective yet undrilled area in the SW sector (marked by a red circle) (Fig. 9 and 10) necessitates further investigation with comprehensive well logs for accurate reservoir assessment. Faults act as critical seals, particularly where sweetness diminishes near shale-prone intervals. A promising gas accumulation (red rectangle) in the central seismic section is structurally trapped between bounding faults.

Non-porous shoreface clastics overlying the B-Sand exhibit low sweetness, forming an effective regional seal. Underlying channel and point bar deposits, characterized by low GR values, confirm reservoir potential. Three key zones (Fig. 9), two near existing wells and a third prospective area, demonstrate significant hydrocarbon potential, supported by integrated seismic, well-log, and structural analyses.

6.5 Relative Acoustic Impedance (RAI)

The Relative Acoustic Impedance (RAI) attribute has been meticulously mapped along the B-Sand formation within a time interval of 1.30-1.65 seconds and a frequency range of 10-30 Hz (Fig. 11). On this map, red to yellow hues signify the highest impedance values, while dark blue to black indicates the lowest. Variations in acoustic impedance can be influenced by

factors such as porous medium compaction, crystal phase changes, fluid loss from porous media, and temperature reduction due to compression, often exacerbated by the presence of faults. Figure 11 clearly delineates four prominent faults traversing the B-Sand. The eastern and southwestern parts of the map exhibit dark blue values, which are interpreted as shale-dominated zones, indicating non-productive areas. These low impedance values are likely attributed to the presence of water-bearing shales.

An RAI seismic section generated along Inline No. 71 (Fig. 12) further elucidates the study area's structural complexity. The application of the RAI attribute effectively highlights fault surfaces, revealing zones within the B-Sand where faulting has led to compaction and localized loss of pore space. These faults are characterized by a step-faulting geometry, trending from Northwest (NW) to Southeast (SE). Changes in acoustic impedance are also directly linked to variations in seismic velocity; a decrease in velocity, typically observed when seismic waves traverse less dense or faulted zones, results in a corresponding reduction in acoustic impedance.

Stratigraphically, the zone of interest primarily comprises shelfal and deltaic paralic sequences that define the Lower Goru Member. The sand-prone sequences within the Lower Goru are highly prospective, consisting of sandstones interbedded with shale beds. These units were deposited in various settings, including strand plains, deltaic marine environments, and barrier bar shoreface to offshore ramp settings.

Through the integrated analysis of reflection configurations, the RAI attribute, and data from the two wells (Jumman Shah-01 and Dars West-01), it is noted that the mapped channels are predominantly filled with sandy beds exhibiting relatively high impedance (red color). Conversely, the shaly interbeds show low impedance (black color). The B-Sand interval itself is encased by shale beds, specifically the Upper Goru Formation above and the Badin Shale below (Fig. 12). These characteristic features collectively indicate the presence of high-quality potential stratigraphic hydrocarbon reservoirs within the sandstone units.

6.6 Trace Envelope (TE)

The TE attribute has been sliced along the B-Sand formation (Fig. 13) to meticulously investigate variations in channel body geometry. This attribute horizon slice distinctly reveals well-developed meandering channels exhibiting high to medium asymmetry, separated by a few meters, as delineated by the red lines. This morphology suggests deposition in a moderate to high-energy nearshore sedimentary environment, likely influenced by fluctuating sea levels.

The TE attribute displayed on seismic In-line 71 (Fig. 14) clearly highlights acoustic impedance contrast and, consequently, reflectivity. High TE values are depicted in red-yellow, while low values appear in blue-black. The presence of gas sands within this formation is evidenced by high reflectivity (red coloration), with darker red tones indicating significant gas accumulation in the B-Sand where the Jumman Shah-01 and Dars West-01 wells are drilled. This gas accumulation is further supported by the presence of faults within the B-Sand, which act as perfect seals and traps. These high TE values also correlate with zones of inferred high porosity and permeability. Conversely, low TE values above and below the B-Sand formation signify non-porous and non-productive zones, indicative of interbedded sand and shale sequences. An additional zone, highlighted by a red circle and rectangle in Figs. 13 and 14, respectively, also suggests hydrocarbon accumulation. As this area remains undrilled, it warrants future consideration for comprehensive well logging to accurately quantify its hydrocarbon potential.

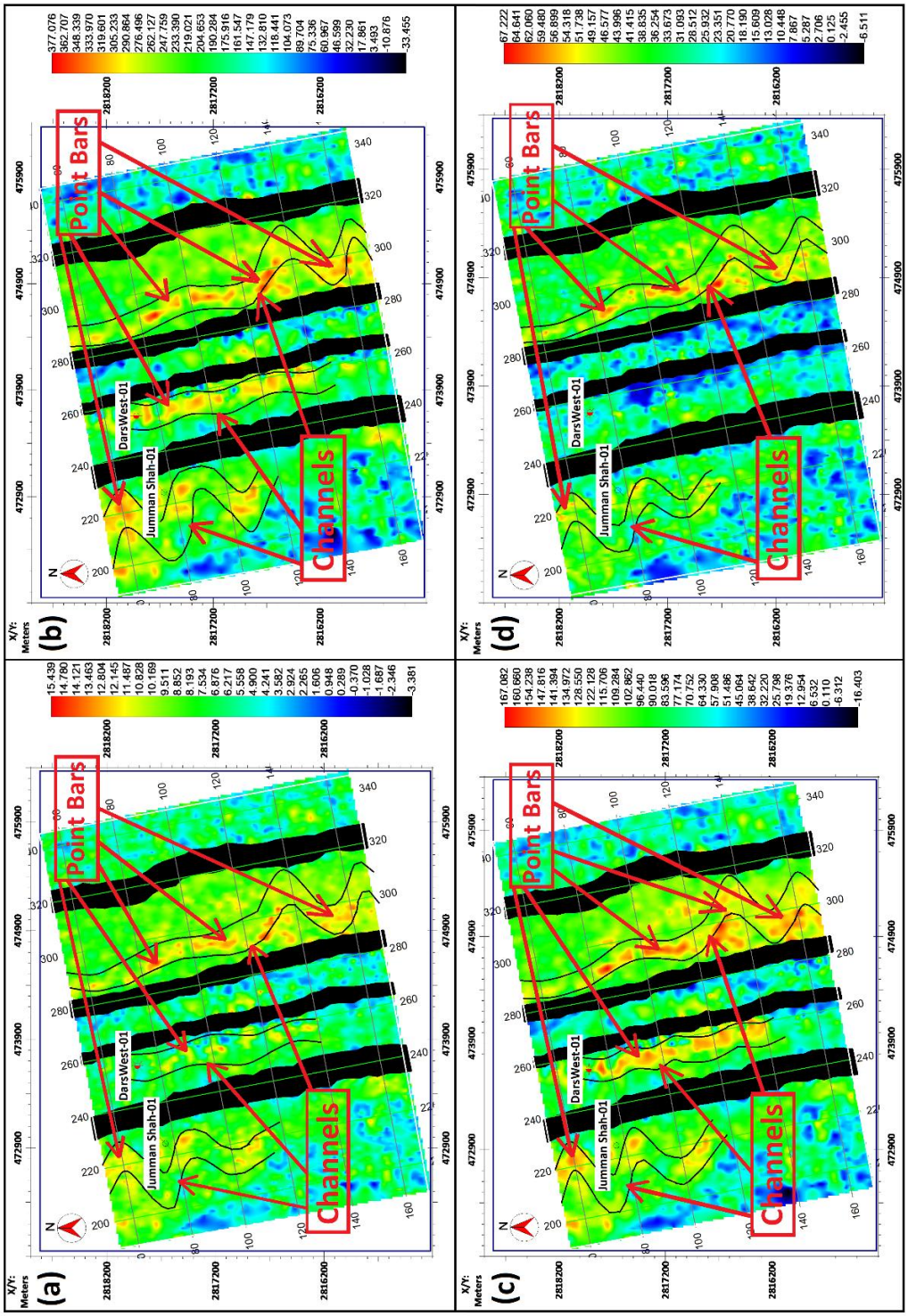

Fig. 8. Seismic attribute analysis of the B-Sand sequence **(a)** Sweetness, **(b)** RAI, **(c)** TE, **(d)** RMS reveals diverse channel morphologies (point bars, straight and sinuous meandering) and suggests potential lithology variations based on impedance contrasts.

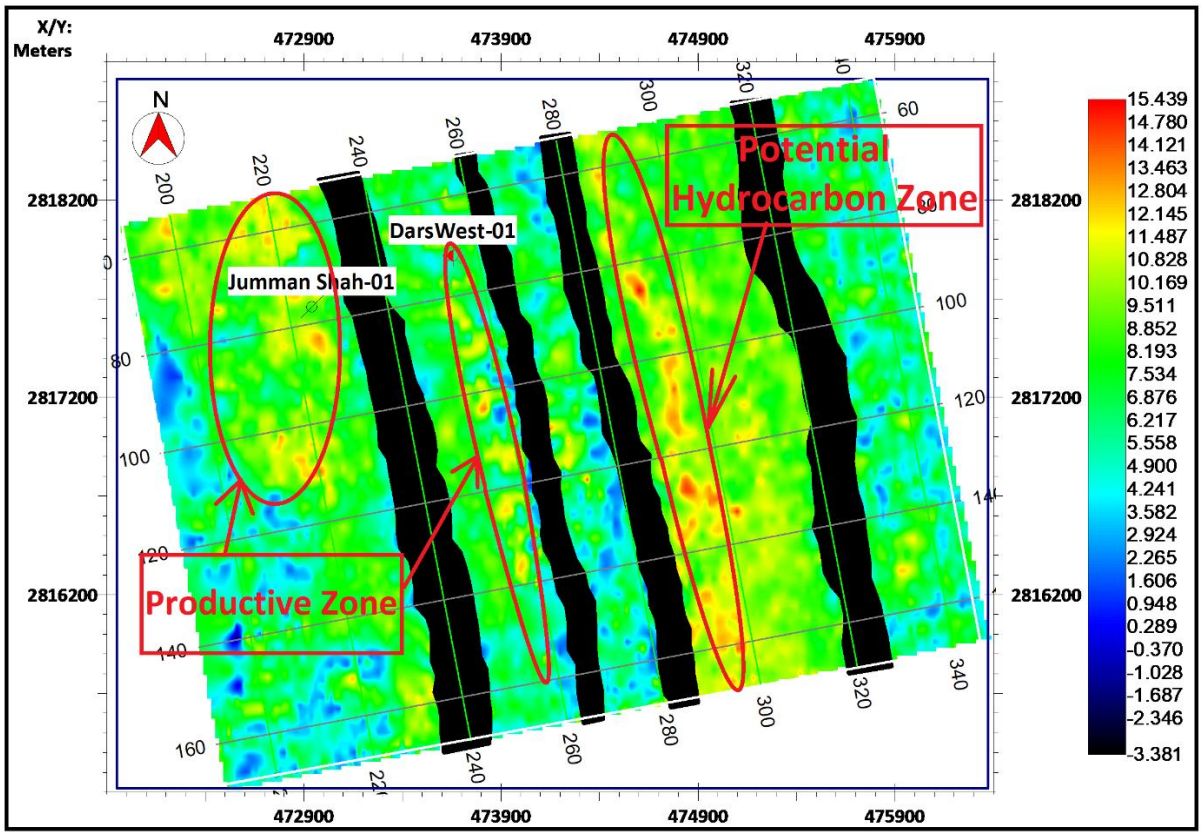

Fig. 9. The Relative Acoustic Impedance Attribute Extracted Along the Horizon Corresponding to the B-Sand Reservoir.

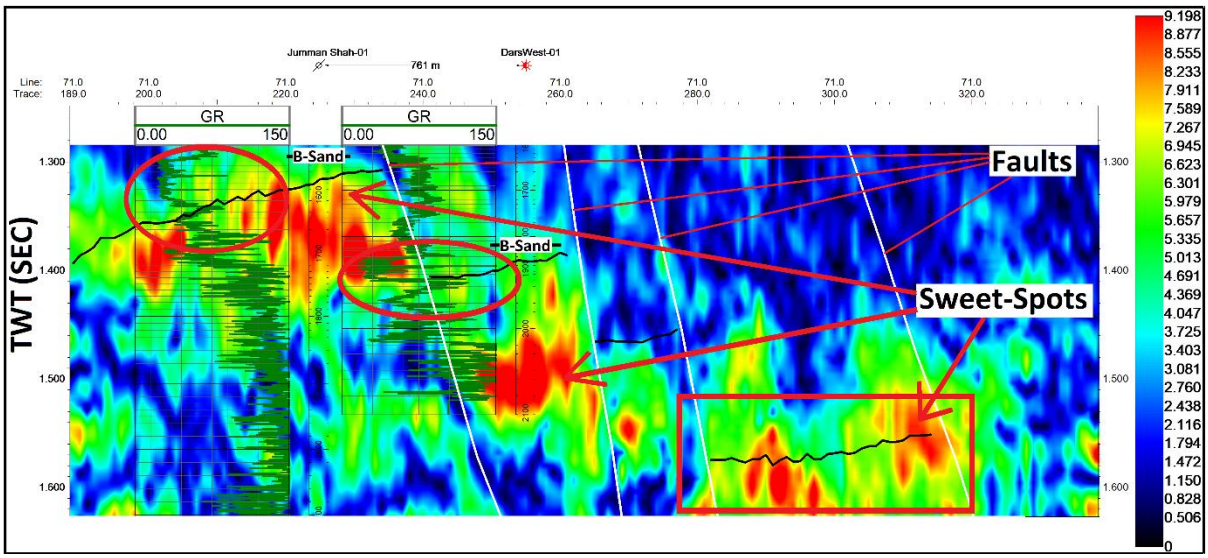

Fig. 10. The Sweetness attribute on seismic Inline No. 71 highlights three sweet spots, generated with a 10-30 Hz frequency range, and four faults (Fault-1 to Fault-4).

6.7 Root Mean Square (RMS)

The Root Mean Square (RMS) amplitude attribute, applied to the B-Sand formation as shown in Figure 15, effectively delineates zones of moderate to high amplitude. These amplitude variations indicate a reservoir primarily composed of sand, with some interbedded thin shale layers, suggesting good to fair porosity within the sandy intervals. Given that the study area largely comprises gas-bearing wells, these high-amplitude zones are

interpreted as areas of significant gas accumulation.

Observation from the RMS Amplitude analysis (Fig. 15) further corroborates the presence of an underexplored, high-potential hydrocarbon zone. This prospective area is situated within the downthrown block of a major normal fault and is highlighted by a red circle on the map (Fig. 15).

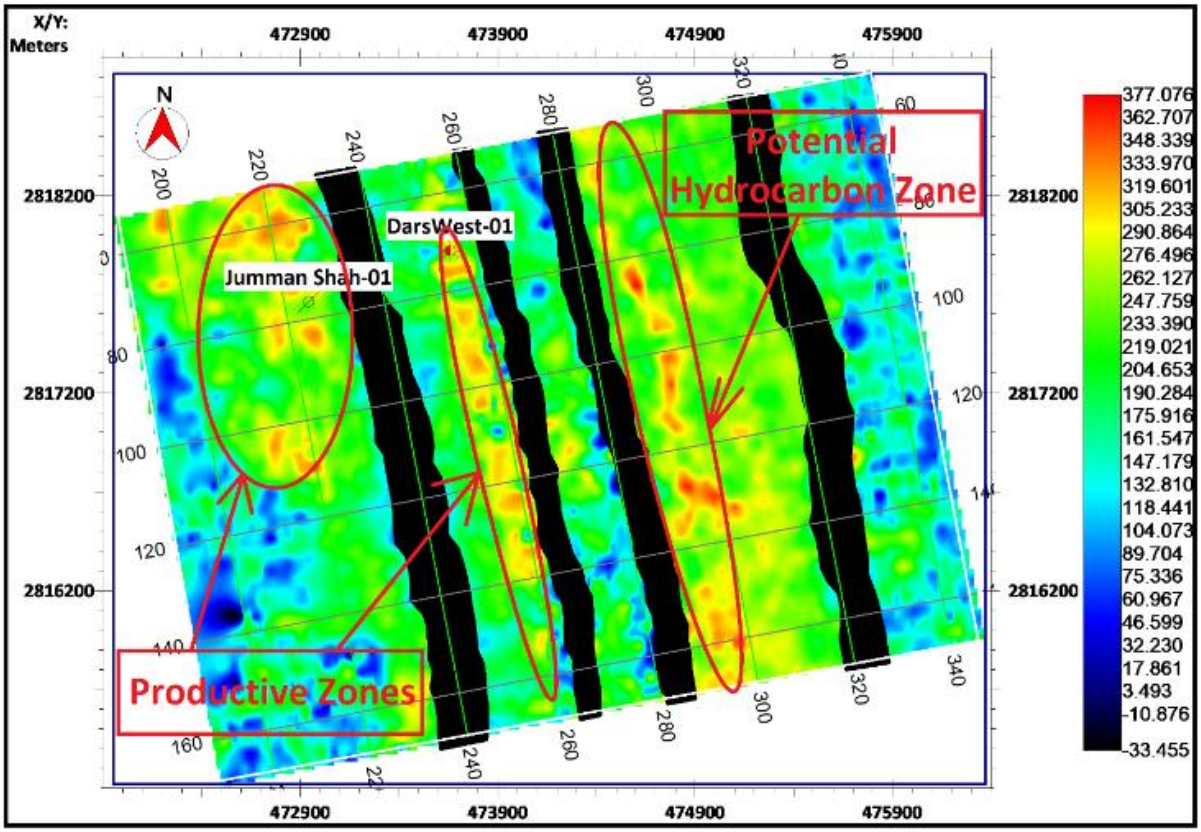

Fig. 11. Extracted Relative Acoustic Impedance Attribute along the Horizon of B-Sand.

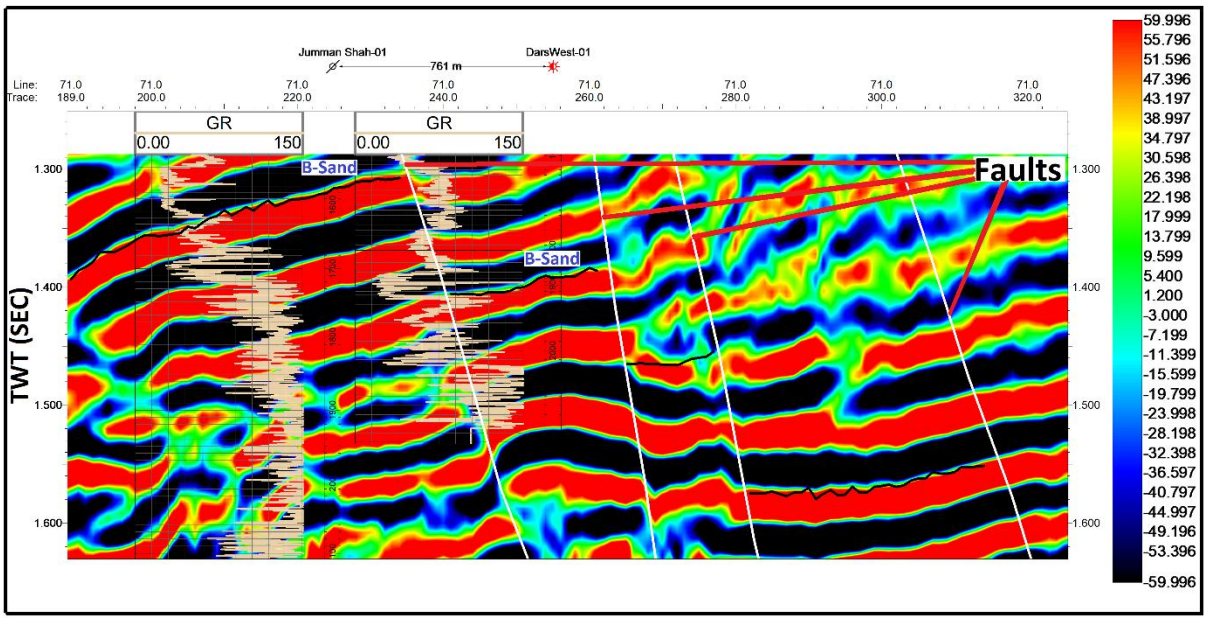

Fig. 12. The RAI attribute on seismic Inline No. 71 highlights faulted zones (Fault-1, Fault-4) with step faulting structures, generated with a 10-30 Hz frequency range.

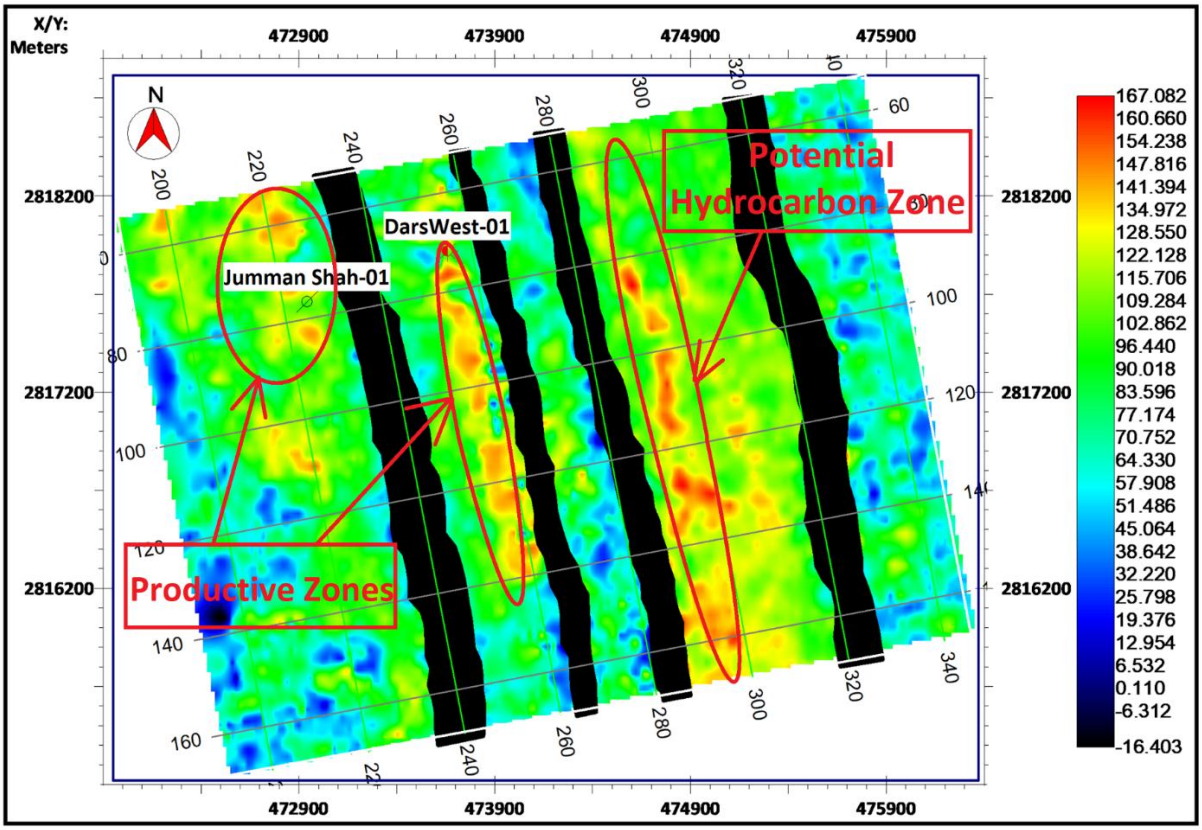

Fig. 13. The Trace Envelope Attribute Extracted Along the Horizon Corresponding to the B-Sand Layer.

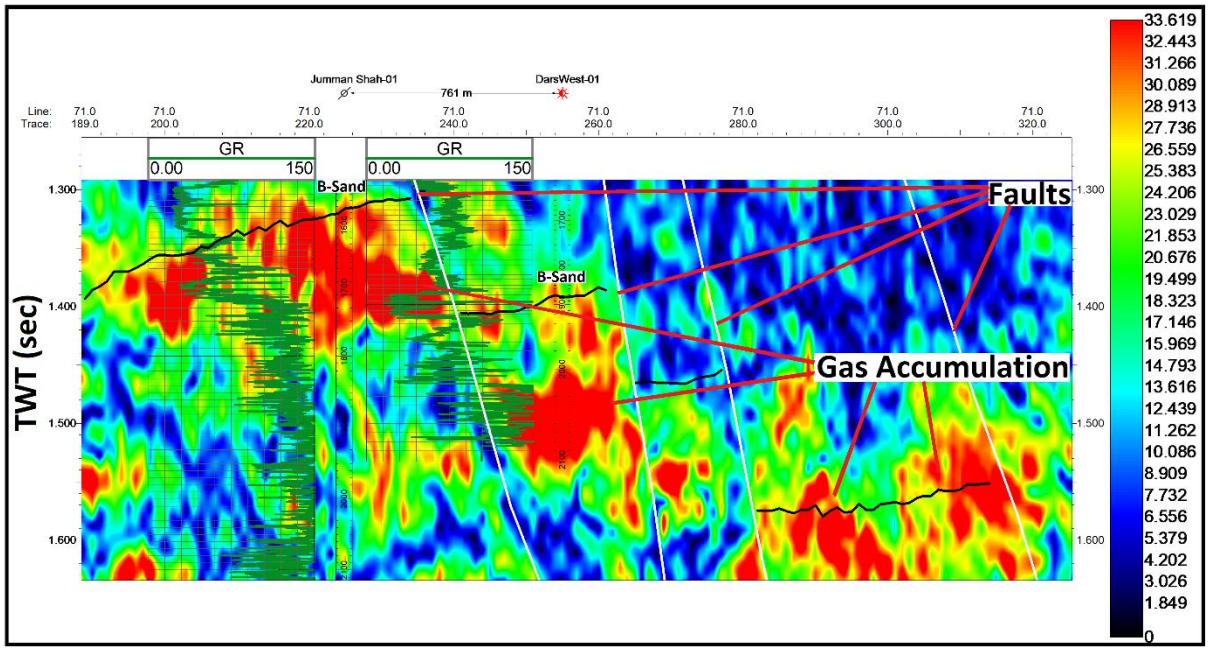

Fig. 14. The Trace Envelope attribute on seismic Inline No. 71 (Fig. 2) highlights faulted zones (Fault-1 to Fault-4) with step faulting structures, generated with a 10-30 Hz frequency range.

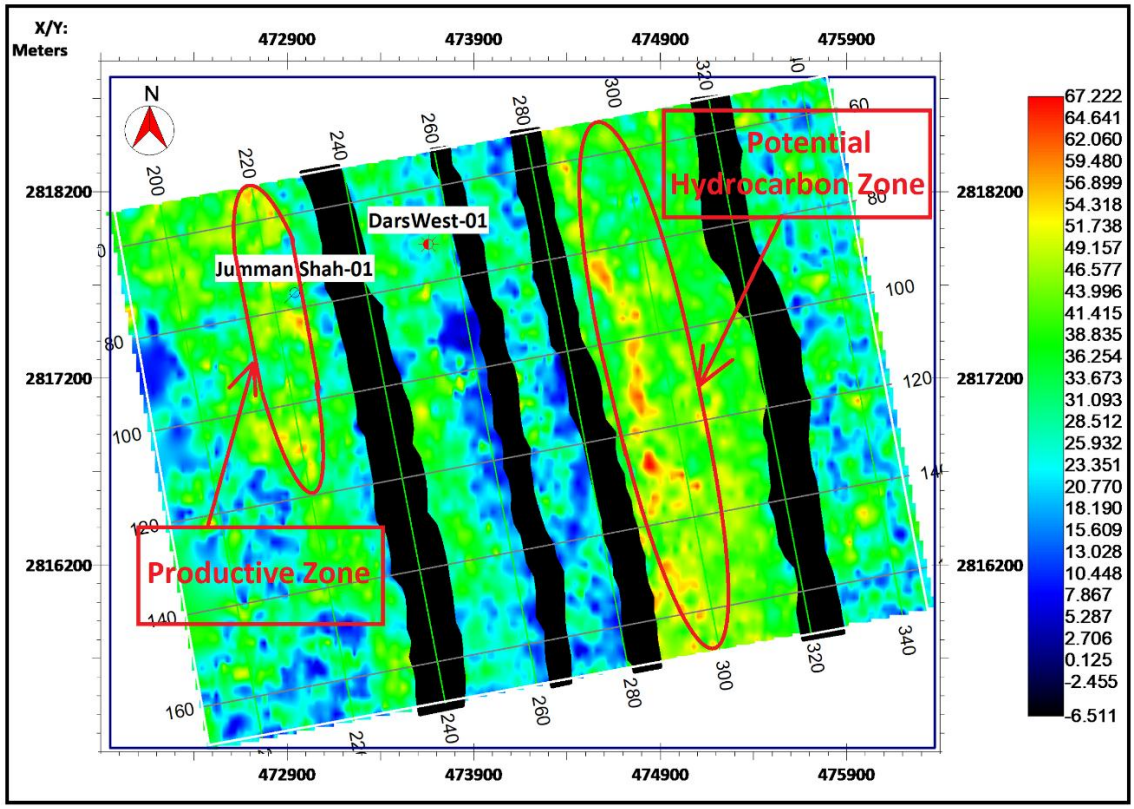

Fig. 15. The Root Mean Square (RMS) Attribute Extracted along the B-Sand Horizon, with the Potential Hydrocarbon Zone Highlighted by a Circle.

7. Discussion

This study comprehensively evaluates the petroleum prospectivity of the B-Sand unit, located within the Upper Sands of the Lower Goru Formation in the NIM exploration block, Pakistan (Fig. 1). The aim is to ascertain its production potential and identify promising prospect zones for future research. This evaluation involved an integrated approach utilizing petrophysics, well log analysis, seismic attributes, and seismic inversion.

The seismic data for the B-Sand unit clearly indicate the influence of extensional tectonics, resulting in regional-scale normal fault structures (Fig. 4). These geological structures are interpreted as forming highly effective traps within the study area, significantly enhancing the likelihood of hydrocarbon discoveries in such structural traps. Furthermore, the research area's location within the mature petroleum play of the Sembar and Lower Goru Formations (Wandrey et al., 2004) further elevates its exploration potential.

A thorough petrophysical examination was conducted on the two wells provided for the B-Sand reservoir unit within the study area. Key petrophysical parameters, including porosity, shale volume, water saturation, and hydrocarbon saturation, were meticulously estimated and interpreted for the reservoir interval. The petrophysical analysis confirms the B-Sand unit as the primary gas-producing reservoir in the studied region (Figs. 6 and 7). Correlation with well data aided in identifying promising sand zones with high reservoir quality in existing wells. While well Jumman Shah-01 exhibits strong porosity indicators, its high-water content (water saturation of 79%) significantly limits its hydrocarbon holding capacity (Fig. 6). Conversely, Dars West-01, located in a deeper section of the target reservoir, shows encouraging hydrocarbon

indicators (hydrocarbon saturation of 56% vs. 20% in Jumman Shah-01), despite still being water-wet (water saturation of 43%) (Fig. 7). Both wells demonstrate reasonable to good effective porosity (approximately 11% in Jumman Shah-01 and 17% in Dars West-01) with low shale volumes (18% and 20% respectively).

This integrated approach, combining petrophysics and seismic attribute analysis, proved highly effective in identifying prospective hydrocarbon locations and mapping the lateral distribution of good-quality sands. The study demonstrates that a joint examination of seismic attributes with petrophysical data can significantly aid in predicting unexploited zones within already developed fields. Specifically, seismic attributes are well-suited for delineating lithofacies distribution, channel identification, and prospect zone definition within the basin. Figs. (9, 11, 13, and 15) display moderate to high attribute values, highlighting the presence of sand bodies and providing detailed insights into hydrocarbon-producing and potential zones. The placement of Jumman Shah-01 and Dars West-01 within these moderate to high amplitude zones suggests that the reservoir sandstones were likely deposited in a shoreface environment (Blanke, 2013; Sahoo et al., 2014). These figures further indicate that non-productive sand/shale intervals formed during transgressive periods, whereas gas-producing sands were likely deposited during regressive phases. High amplitude attribute values in these zones suggest that the reservoir is highly interbedded with thin laminated shale layers, while the lowest values indicate relatively thicker gas-bearing sand reservoirs.

Seismic attributes generated from seismic data (Figs. 10, 12, and 14) were crucial for investigating both lateral and vertical variations within the B-Sand. The findings show that both wells are situated near shelf edge deltas that hit the desired sweet spot zone (Fig. 14), and these sweet spot zones are bounded by the low sweetness zones. There is also a possibility shown from the sweet spot attribute that the shoreface lowstand system tract gas producing sand was deposited on the distal shaly and silty sediment of the highstand system tract which, was sealed by transgressive shales and siltstones (Fig. 14). However, one more sweet spot can also be seen in Figure 14 (shown by rectangle) which seems to be an area favorable for hydrocarbon exploration.

8. Conclusions

This study presents an integrated geophysical analysis of the B-Sand reservoir in the NIM exploration Block, combining well log facies and 3D seismic attribute analysis. The B-Sand, characterized by interbedded sandstones and shales from a fluvial-dominated deltaic system, was thoroughly investigated. Seismic attributes like Sweetness, TE, RAI, and RMS were crucial in identifying subtle structures, faults, and hydrocarbon "sweet spots," providing insights beyond traditional seismic interpretation. The positive amplitude anomaly of the B-Sand indicates hydrocarbon accumulation, and the faults are recognized for their role in both trapping and migration. This comprehensive approach significantly reduces exploration risks and aids in better reservoir characterization and future drilling strategies.

Acknowledgments

The authors would like to acknowledge Landmark Resources for providing the data, and also to the Director General of Petroleum Concessions (DGPC) for helping out in getting the data provided.

Author's Contribution

Furqan Mahmud Butt was responsible for the comprehensive interpretation of the data, encompassing petrophysical and seismic attribute analyses, and for authoring this research paper. Umair Bin Nisar provided rigorous validation and a detailed analytical review of the presented findings. The entire research endeavor, including all analyses, was conducted under the expert supervision

of Shazia Naseem. The authors declare no conflict of interest or competing interests in this work.

Funding: Not Applicable

Data availability

The datasets used and/or analyzed during the study are available on request from the corresponding author.

DECLARATIONS

Conflict of interest: The authors declare no competing interests.

Ethics approval and consent to participate.

The authors declare that they followed the ethics in scientific research.

Consent for publication.

Not applicable

Competing interests

The authors declare no competing interests.

Conflict of interests: The authors reported no potential conflict of interest.

References

Abbasi, S. A., Solangi, S. H., & Ali, A. (2015a). Seismic data interpretation: A case study of Southern Sindh Monocline, Lower Indus Basin, Pakistan. *Mehran University Research Journal of Engineering and Technology*, *34*(2), 107–115.

Abbasi, S. A., Solangi, S. H., Nazeer, A., Asim, S., Habib, W., & Solangi, I. A. (2015b). An overview of structural style and hydrocarbon potential of Jabo Field, Southern Sindh Monocline, Southern Indus Basin. *Sindh University Research Journal (Science Series)*, *47*(2), 347–354.

Ahmed, S. (2018). *Study of tectonic evolution of structures and their hydrocarbon potential using seismic data, Southern Sindh Monocline, Pakistan* [Doctoral dissertation, University of Sindh, Jamshoro].

Ahmed, S., Solangi, S. H., Brohi, I. A., Khokhar, Q. D., & Lashari, R. A. (2014). Study of stratigraphy and structural styles in the subsurface of Southern Sindh Monocline, Pakistan: Using seismic and well data. *Sindh University Research Journal (Science Series)*, *46*(4), 439-446.

Ahmed, S., Solangi, S. H., Jadoon, M. S. K., & Nazeer, A. (2018). Tectonic evolution of structures in the Southern Sindh Monocline, Indus Basin, Pakistan formed in multi-extensional tectonic episodes of Indian Plate. *Geodesy and Geodynamics*, *9*(5), 358–366.

Ali, A., Alves, T. M., Saad, F. A., Ullah, M., Toqeer, M., & Hussain, M. (2018). Resource potential of gas reservoirs in South Pakistan and adjacent Indian subcontinent revealed by post-stack inversion techniques. *Journal of Natural Gas Science and Engineering*, *49*, 41-55.

Alsouki, M., Taifour, R., & Al Hamad, O. (2014). Delineating the fluvial channel system in the Upper Triassic formation of the Elward area in the Syrian Euphrates Graben using 3-D seismic attributes. *Journal of Petroleum Exploration and Production Technology*, *4*(2), 123–132.

Anees, A., Shi, W., Ashraf, U., & Xu, Q. (2019). Channel identification using 3D seismic attributes and well logging in Lower Shihezi Formation of Hangjinqi area, northern Ordos Basin, China. *Journal of Applied Geophysics*, *163*, 139–150.

Archie, G. E. (1952). Classification of carbonate reservoir rocks and petrophysical considerations. *American Association of Petroleum Geologists Bulletin*, *36*(2), 278–298.

Asquith, G. B., & Gibosn, C. R. (1982). *Basic well log analysis for geologists*. American Association of Petroleum Geologists.

Asquith, G. B., Krygowski, D., & Gibson, C. R. (2004). *Basic well log analysis* (Vol. 16). American Association of Petroleum Geologists.

Azeem, T., Chun, W. Y., MonaLisa, Khalid, P., Qing, L. X., Ehsan, M. I., & Wei, X. (2017). An integrated petrophysical and rock physics analysis to improve reservoir

characterization of Cretaceous sand intervals in Middle Indus Basin, Pakistan. *Journal of Geophysics and Engineering*, *14*(2), 212-225.

Azeem, T., Yanchun, W., Khalid, P., Xueqing, L., Yuan, F., & Lifang, C. (2016). An application of seismic attributes analysis for mapping of gas bearing sand zones in the Sawan Gas Field, Pakistan. *Acta Geodaetica et Geophysica*, *51*(4), 723–744.

Baig, M. O., Harris, N. B., Ahmed, H., & Baig, M. O. A. (2016). Controls on reservoir diagenesis in the Lower Goru sandstone formation, Lower Indus Basin, Pakistan. *Journal of Petroleum Geology*, *39*(1), 29–47.

Barnes, A. E. (Ed.). (2016). *Handbook of poststack seismic attributes*. Society of Exploration Geophysicists.

Beaumont, E. A., & Foster, N. H. (Eds.). (1999). *Exploring for oil and gas traps* (Vol. 3). American Association of Petroleum Geologists.

Bilal, A., Mughal, M. S., Janjuhah, H. T., Ali, J., Niaz, A., Kontakiotis, G., & Yang, R. (2022). Petrography and provenance of the Sub-Himalayan Kuldana Formation: Implications for tectonic setting and Palaeoclimatic conditions. *Minerals*, *12*(7), 794-820.

Blanke, S. J. (2013). Saucer sills of the offshore Canterbury Basin. In *Advantage NZ Petroleum Conference*. Auckland.

Bridge, J. S., & Tye, R. S. (2000). Interpreting the dimensions of ancient fluvial channel bars, channels, and channel belts from wireline-logs and cores. *American Association of Petroleum Geologists AAPG Bulletin*, *84*(8), 1205–1228.

Brown, A. R. (2011). *Interpretation of three-dimensional seismic data*. Society of Exploration Geophysicists and American Association of Petroleum Geologists.

Chopra, S., & Marfurt, K. J. (2013). Structural curvature versus amplitude curvature. *The Leading Edge*, *32*(2), 178-184.

Daber, R., Aqrawi, A., Larsen, C., Boe, T. H., Pepper, R., Barros, S., & Scollard, A. (2007). *Interpreters' guide to seismic attributes*. Schlumberger.

Dake, L. P. (1983). *Fundamentals of reservoir engineering* (Vol. 8). Elsevier.

Dorn, G. A. (1999). Treatise of petroleum geology/Handbook of petroleum geology: Exploring for oil and gas traps. *American Association of Petroleum Geologist*.

Ehsan, M., Gu, H., Ali, A., Akhtar, M. M., Abbasi, S. S., Miraj, M. A. F., & Shah, M. (2021). An integrated approach to evaluate the unconventional hydrocarbon generation potential of the Lower Goru Formation (Cretaceous) in Southern Lower Indus basin, Pakistan. *Journal of Earth System Science*, *130*(2), 90.

Emujakporue, G. O., & Enyenihi, E. E. (2020). Identification of seismic attributes for hydrocarbon prospecting of Akos field, Niger Delta, Nigeria. *SN Applied Sciences*, *2*, 1–11.

Hart, B. S. (2008). Channel detection in 3-D seismic data using sweetness. *American Association of Petroleum Geologists Bulletin*, *92*(6), 733–742.

Hart, B. S., & Balch, R. S. (2000). Approaches to defining reservoir physical properties from 3-D seismic attributes with limited well control: An example from the Jurassic Smackover Formation, Alabama. *Geophysics*, *65*(2), 368–376.

Hong, Y., Wang, H., Tian, W., & Mo, A. (2013). Identification and prediction of the high heterogeneous channel sand in Southern Turgay Basin. In *AAPG Annual Convention and Exhibition* (p. 10515). Pittsburgh, Pennsylvania: American Association of Petroleum Geologists.

Khalid, P., & Ghazi, S. (2013). Discrimination of fizz water and gas reservoir by AVO analysis: A modified approach. *Acta Geodaetica et Geophysica*, *48*(3), 347–361.

Khalid, P., Ehsan, M. I., Akram, S., Din, Z. U., & Ghazi, S. (2018). Integrated reservoir characterization and petrophysical analysis of Cretaceous sands in Lower Indus Basin,

Pakistan. *Journal of the Geological Society of India*, *92*(4), 465–470.

Khalid, P., Qayyum, F., & Yasin, Q. (2014). Data-driven sequence stratigraphy of the Cretaceous depositional system, Punjab Platform, Pakistan. *Surveys in Geophysics, 35*, 1065-1088.

Knight, B., Capitanio, F. A., Weinberg, R. F., & Dal Zilio, L. (2023). India-Asia slowing convergence rate controls on the Cenozoic Himalaya-Tibetan tectonics. *Authorea Preprints*.

Krois, P., Mahmood, T., & Milan, G. (1998, November). Miano field, Pakistan, A case history of model driven exploration. In *Proceedings Pakistan petroleum convention* (Vol. 98, pp. 112-131). Pakistan Association of Petroleum Geoscientists (PAPG), Islamabad, Pakistan.

Mehana, M., & El-monier, I. (2016). Shale characteristics impact on Nuclear Magnetic Resonance (NMR) fluid typing methods and correlations. *Petroleum*, *2*(2), 138–147.

Owolabi, A. O., Omang, B. O., Oyetade, O. P., & Akindele, O. B. (2019). Reservoir evaluation and volumetric analysis of Rancho Field, Niger Delta, using well log and 3D seismic data. *Open Journal of Geology*, *9*(13), 974.

Raef, A. E., Mattern, F., Philip, C., & Totten, M. W. (2015). 3D seismic attributes and well-log facies analysis for prospect identification and evaluation: interpreted palaeoshoreline implications, Weirman Field, Kansas, USA. *Journal of Petroleum Science and Engineering*, *133*, 40-51.

Sahoo, T. R., Browne, G. H., & Hill, M. G. (2014). Seismic attribute analysis and depositional elements in the Canterbury Basin. In *Poster presented at the Advantage NZ: Geotechnical Petroleum Forum*.

Sanguinetti, R. (2006). Image processing techniques applied to 3-D attribute volumes for lithology distribution. In *SEG Technical Program Expanded Abstracts 2006* (pp. 1806-1810). Society of Exploration Geophysicists.

Schenk, C. J., Tennyson, M. E., Klett, T. R., Finn, T. M., Mercier, T. J., Gaswirth, S. B., Marra, K. R., Le, P. A., Hawkins, S. J., & Leathers-Miller, H. M. (2017). *Assessment of undiscovered oil and gas resources in the Lower Indus Basin, Pakistan, 2017* (No. 2017-3034). US Geological Survey.

Taner, M. T. (2001). Seismic attributes. *Canadian Society of Exploration Geophysicists (CSEG) Recorder*, *26*(7), 49–56.

Taner, M. T., Koehler, F., & Sheriff, R. E. (1979). Complex seismic trace analysis. *Geophysics*, *44*(6), 1041–1063.

Wandrey, C. J., Law, B. E., & Shah, H. A. (2004). *Sembar Goru/Ghazij composite total petroleum system, Indus and Sulaiman-Kirthar geologic provinces, Pakistan and India* (No. 2208-C).

Wyllie, M. R. J., Gregory, A. R., & Gardner, L. W. (1956). Elastic wave velocities in heterogeneous and porous media. *Geophysics*, *21*(1), 41–70.

Zahmatkesh, I., Kadkhodaie, A., Soleimani, B., Golalzadeh, A., & Azarpour, M. (2018). Estimating Vsand and reservoir properties from seismic attributes and acoustic impedance inversion: A case study from the Mansuri oilfield, SW Iran. *Journal of Petroleum Science and Engineering*, *161*, 259–274.

Zehra, S., & Afsar, S. (2016). Flood hazard mapping of Lower Indus Basin using Multi-Criteria Analysis. *Journal of Geoscience and Environment Protection*, *4*(4), 54-62.

Zhang, J. H., Liu, Z., Zhu, B. H., Feng, D. Y., Zhang, M. Z., & Zhang, X. F. (2011). Fluvial reservoir characterization and identification: A case study from Laohekou Oilfield. *Applied Geophysics*, *8*(3), 181–188.